

DETC2004/MECH-57455

DESIGN OPTIMIZATION FOR A PARALLEL MEMS MECHANISM WITH FLEXURE JOINTS

Byoung Hun Kang

Mechanical, Aerospace and Nuclear Engineering
Rensselaer Polytechnic Institute
110 8th Street CII 8015
Troy, NY, 12180
Email: robot@alum.rpi.edu

John T. Wen

Mechanical, Aerospace and Nuclear Engineering
Electrical, Computer and Systems Engineering
Rensselaer Polytechnic Institute
110 8th Street CII 8015
Troy, NY, 12180
Email: wen@cat.rpi.edu

Nicholas G. Dagalakis

Intelligent Systems Division
National Institute of Standards and Technology
100 Bureau Drive, Mail Stop 8230
Gaithersburg, MD 20899
Email: nicholas.dagalakis@nist.gov

Jason J. Gorman

Intelligent Systems Division
National Institute of Standards and Technology
100 Bureau Drive, Mail Stop 8230
Gaithersburg, MD 20899
Email: gorman@cme.nist.gov

ABSTRACT

This paper presents an analysis tool and design method for MEMS parallel mechanisms. Due to processing constraints in MEMS fabrication, flexure joints are frequently used in MEMS mechanisms. Flexure joints offer advantages over other joint design due to their monolithic characteristics. They can be used to reduce the size of manipulators or to increase the precision of motion. Their inherent flexibility, however, also results in task space compliance which needs to be carefully designed to match the task specification. This paper presents an analysis and design tool for such mechanisms by using the differential kinematics. Performance metrics are chosen based on manipulability and task stiffness matrices, which in turn are used in a multi-objective optimization. As an illustrative example, a 1-DOF MEMS parallel mechanism based on the macro- and meso-scale models designed by NIST is considered with several choices of performance metrics and design variables. The resulting designs are successfully fabricated using DRIE process.

NOMENCLATURE

- Δx_T spatial velocity in the Cartesian space.
- Δx_C constraint velocity in the Cartesian space.
- f_T spatial force in the Cartesian space.
- f_C constraint force in the Cartesian space.
- Δq_a active joint velocity in the joint space.
- Δq_p passive joint velocity in the joint space.
- τ_a active joint torque in the joint space.
- τ_p passive joint torque in the joint space.
- J_{Ta} mapping between the spatial and the active joint velocity.
- J_{Tp} mapping between the spatial and the passive joint velocity.
- J_{Ca} mapping between the constraint and the active joint velocity.
- J_{Cp} mapping between the constraint and the passive joint velocity.
- K_T spatial stiffness matrix in the Cartesian space.
- K_q joint stiffness matrix in the joint space.
- \tilde{A} annihilator of matrix A ($\tilde{A}A = 0$).

INTRODUCTION

Due to the limitation of micro-fabrication processes, flexure joints are frequently used in micro-electro-mechanical-systems (MEMS) mechanisms. In general, for precision mechanisms with limited motion range, flexure joints offer significant advantages over conventional joints [1, 2] in terms of both manufacturability and operational characteristics. Flexure joints are typically manufactured monolithically and therefore avoid assembly errors. The monolithic construction also implies potentially very compact design. In terms of operation, flexure joints have low friction losses, do not require lubrication, and generate smooth and continuous displacement without backlash. With a suitable choice of material, flexure joints exhibit a predictable and repeatable relationship between force and displacement.

Due to the inherent flexibility of the joints, a MEMS mechanism with flexure joints will exhibit certain task space compliance. To ensure compatibility with a given task specification, the MEMS mechanism needs to be carefully designed to balance between the motion objective (manipulability) and the load bearing objective (stiffness) subject to the maximum stress constraints. As a result, in addition to the geometric parameters, the design variables will also contain the joint characteristics in order to meet the task space stiffness objective.

Thorough treatments of the characterization and design of flexure joints and mechanisms may be found in [1, 3]. Flexure mechanism design is usually addressed either from a kinematic synthesis point of view with the overall mechanism compliance as a secondary criterion, or from the compliance point of view [1] with the emphasis on synthesizing desired compliance characteristics using, for example, topological optimization [4, 5] or finite element analysis [6, 7]. The general problem of compliance synthesis has been addressed using simple springs [8] with specific solutions proposed for torsional and line springs in [9–11]. However, such approaches have several drawbacks: the design criterion only involves the desired compliance; constraints are not taken into account; and the overall mechanism is passive without consideration of actuators. The specific problem of synthesizing a desired grasp compliance by choosing appropriate finger compliance is used in [12]. Independent of joint compliance, optimization based design methods have also been developed for parallel mechanisms [13, 14], but the joint compliance is not taken into account. A well established criterion for assessing the behavior of a serial or parallel manipulator is the manipulability ellipsoid which is the task space image of a ball in the active joint velocity space. This concept was first proposed for serial manipulators [15] and later extended to parallel robots [16, 17].

The goal of this paper is to present analysis and design tools for parallel mechanisms containing flexure joints based on the pseudo-rigid-body model. Our approach is to balance the motion and compliance consideration through a multi-objective optimization. The Pareto frontier [18] is calculated and the final design is determined based on secondary considerations such as

dynamic characteristics and performance sensitivity. As an example, we include the MEMS design based on the macro- and meso-scale versions of a 1-D stage designed by the National Institute of Standards and Technology (NIST). Several choices of performance metrics and design variables are considered to illustrate the design approach described in this paper.

DIFFERENTIAL KINEMATICS

Consider a parallel mechanism with active and passive joints. The differential kinematics, the velocity mapping between joint space and Cartesian space, of general multibody systems may be described as

$$\begin{bmatrix} \Delta x_T \\ 0 \end{bmatrix} = \underbrace{\begin{bmatrix} J_{T_a} & J_{T_p} \\ J_{C_a} & J_{C_p} \end{bmatrix}}_{J := \begin{bmatrix} J_T \\ J_C \end{bmatrix}} \underbrace{\begin{bmatrix} \Delta q_a \\ \Delta q_p \end{bmatrix}}_{\Delta q} \quad (1)$$

Depending on the number of passive joints and that of kinematic constraints, a parallel mechanism can be divided into three different cases.

For parallel mechanisms with conventional passive joints, the mechanism may have the same number of passive joints as kinematic constraints. Therefore, J_{C_p} is typically square so that there is no undesirable internal constraint forces. It is also essential to ensure that J_{C_p} is invertible so there would not be undesired motion. This is known as the kinematic stability condition.

If the number of kinematic constraints is larger than that of the passive joints, J_{C_p} is a tall matrix and the mechanism is overconstrained. It means that the mechanism cannot move unless some of the constraints are redundant. If this is the case for a working mechanism, the rigid body kinematic description is not adequate, and either more lumped joints need to be added or a distributed description should be used.

If there are more passive joints than the kinematic constraints, J_{C_p} is a fat matrix and the mechanism is underconstrained. For conventional parallel mechanisms, this is not desirable, since there could be uncontrolled motion resulting from disturbances. However, we shall see that for flexure mechanisms, this may be acceptable provided that the stiffness in the direction of unwanted motion is sufficiently large.

In this paper, we consider a fully constrained mechanism and an underconstrained mechanism, i.e., J_{C_p} is square or fat. If J_{C_p} is a fat matrix, Δq_p cannot be uniquely solved since any vector in the null space of J_{C_p} may be added to the solution. In this case, we assume that the solution Δq_p minimizes the strain energy in the passive joints where we have assumed linear spring

characteristics with spring constant K_{q_p} :

$$\Delta q_p = -J_{C_p}^\dagger J_{C_a} \Delta q_a. \quad (2)$$

where $J_{C_p}^\dagger$ is the weighted pseudo-inverse of J_{C_p} :

$$J_{C_p}^\dagger := K_{q_p}^{-1/2} (J_{C_p} K_{q_p}^{-1/2})^\dagger. \quad (3)$$

and † denotes the Moore-Penrose pseudo-inverse. If J_{C_p} is square invertible, then $J_{C_p}^\dagger = J_{C_p}^{-1}$.

The relationship between active joint displacement and task displacement in Eqn. (1) is then

$$\Delta x_T = \underbrace{(J_{T_a} - J_{T_p} J_{C_p}^\dagger J_{C_a})}_{:=J_{T_{comp}}} \Delta q_a. \quad (4)$$

By applying the principle of virtual work, we obtain the dual relationship:

$$\underbrace{\begin{bmatrix} \tau_a \\ \tau_p \end{bmatrix}}_{\tau} = \begin{bmatrix} J_{T_a}^T & J_{C_a}^T \\ J_{T_p}^T & J_{C_p}^T \end{bmatrix} \begin{bmatrix} f_T \\ f_C \end{bmatrix}. \quad (5)$$

where f_T is the externally applied spatial force, f_C is the constraint spatial force (to enforce the kinematic constraint, the bottom portion of Eqn. (1)), τ_a and τ_p are the torque vectors applied at the active and passive joints, respectively. When the passive joints are free (e.g., pin, spherical, etc.), $\tau_p = 0$. However, for flexure joints, τ_p is related to Δq_p .

PERFORMANCE MEASURES

For the mechanism design, we need to quantify the performance measure. Differential relationships for parallel mechanisms are shown in Fig. 1, where $x_C (= 0)$ denotes the virtual constraint displacement. We will formulate various performance measures based on these kinematic relationships. Note that, in contrast to parallel mechanisms with conventional joints, kinematic stability is not of paramount importance. Instead, designing the desired stiffness would prevent excessive undesired motion.

We consider the following qualitative motion and stiffness design criteria:

1. The output stage of the mechanism should have a sufficiently large work space in the desired direction of motion and small displacement in the remaining directions.

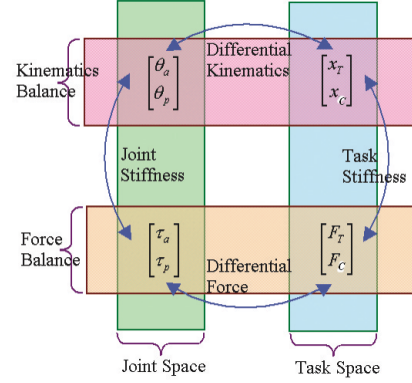


Figure 1. Position and Force Mapping in a General Parallel Mechanism

2. The output stage of the mechanism needs to be sufficiently stiff to avoid undesired motion in the presence of external force.

Based on these criteria, we will choose the performance measures from two classes based on the manipulability matrix and the task space stiffness matrix.

Manipulability

Manipulability is related to the mapping from Δq_a to Δx_T , i.e., $J_{T_{comp}}$, as in Eqn. (4).

Task Space Stiffness

The spatial stiffness in the Cartesian space is defined from the force balance between the applied external spatial force f_T and the corresponding task frame displacement x_T . Similarly, the joint stiffness in the joint space is defined from the torque balance between the overall joint force τ and the corresponding joint displacement q . Using the small deformation assumption, K_T and K_q are constant. Then, the differential relation can be calculated as Eqn. (6).

$$\begin{aligned} \Delta f_T &= K_T \Delta x_T \\ \Delta \tau &= K_q \Delta q \end{aligned} \quad (6)$$

From the equation Eqn. (5), the differential force balance can be rewritten as

$$\Delta \tau = J_{T_a}^T \Delta f_T + J_{C_a}^T \Delta f_C + \Delta J_{T_a}^T f_T + \Delta J_{C_a}^T f_C. \quad (7)$$

By assumption, J_{C_p} is full row rank, therefore, J_C is full row rank. Let \tilde{J}_C be the full column rank matrix whose column space

coincides with the null space of J_C . Then

$$\tilde{J}_C^T \Delta \tau = \tilde{J}_C^T J_T^T \Delta f_T + \tilde{J}_C^T (\Delta J_T^T f_T + \Delta J_C^T f_C). \quad (8)$$

Substituting in Eqn. (6) and using the differential kinematics (top portion of Eqn. (1)), we get

$$\begin{aligned} \tilde{J}_C^T \Delta \tau &= \tilde{J}_C^T J_T^T K_T \Delta x_T + \tilde{J}_C^T (\Delta J_T^T f_T + \Delta J_C^T f_C). \\ &= \tilde{J}_C^T J_T^T K_T J_T \Delta q + \tilde{J}_C^T \left(\Delta J^T \begin{bmatrix} f_T \\ f_C \end{bmatrix} \right). \end{aligned} \quad (9)$$

The derivative of the Jacobian can be calculated as follows:

$$\Delta J^T = \sum_i \frac{\partial J^T}{\partial q_i} \Delta q_i = \sum_i \frac{\partial J^T}{\partial q_{a,i}} \Delta q_{a,i} + \sum_i \frac{\partial J^T}{\partial q_{p,i}} \Delta q_{p,i} \quad (10)$$

The product between ΔJ^T and the spatial and constraint forces is

$$\begin{aligned} \Delta J^T \begin{bmatrix} f_T \\ f_C \end{bmatrix} &= \left(\sum_i \frac{\partial J^T}{\partial q_{a,i}} \Delta q_{a,i} + \sum_i \frac{\partial J^T}{\partial q_{p,i}} \Delta q_{p,i} \right) \begin{bmatrix} f_T \\ f_C \end{bmatrix} \\ &= [\Delta J_{fa}^T \ \Delta J_{fp}^T] \begin{bmatrix} \Delta q_a \\ \Delta q_p \end{bmatrix} \end{aligned} \quad (11)$$

where,

$$\begin{aligned} \Delta J_{fa}^T &= \left[\frac{\partial J^T}{\partial q_{a,1}} (J^T)^+ K_q \begin{bmatrix} q_a \\ q_p \end{bmatrix} : \dots : \frac{\partial J^T}{\partial q_{a,n_a}} (J^T)^+ K_q \begin{bmatrix} q_a \\ q_p \end{bmatrix} \right]. \\ \Delta J_{fp}^T &= \left[\frac{\partial J^T}{\partial q_{p,1}} (J^T)^+ K_q \begin{bmatrix} q_a \\ q_p \end{bmatrix} : \dots : \frac{\partial J^T}{\partial q_{p,n_p}} (J^T)^+ K_q \begin{bmatrix} q_a \\ q_p \end{bmatrix} \right]. \end{aligned}$$

Note that we have assumed that J is of full row. Substituting Eqn. (6) and Eqn. (11) into Eqn. (9), we get

$$\begin{aligned} \tilde{J}_C^T K_q \Delta q &= \tilde{J}_C^T J_T^T K_T \Delta x_T + \tilde{J}_C^T [\Delta J_{fa}^T \ \Delta J_{fp}^T] \begin{bmatrix} \Delta q_a \\ \Delta q_p \end{bmatrix} \\ &= \tilde{J}_C^T J_T^T K_T J_T \Delta q + \tilde{J}_C^T [\Delta J_{fa}^T \ \Delta J_{fp}^T] \Delta q \end{aligned} \quad (12)$$

From the kinematic constraint (bottom portion of Eqn. (1)), we know Δq may be expressed as

$$\Delta q = \tilde{J}_C \phi \quad (13)$$

for some vector ϕ . Substituting into Eqn. (12), we get

$$\tilde{J}_C^T K_q \tilde{J}_C \phi = \tilde{J}_C^T J_T^T K_T J_T \tilde{J}_C \phi + \tilde{J}_C^T [\Delta J_{fa}^T \ \Delta J_{fp}^T] \tilde{J}_C \phi. \quad (14)$$

Since this holds for any ϕ , we obtain the expression for the task space stiffness

$$\tilde{J}_C^T K_q \tilde{J}_C = \tilde{J}_C^T J_T^T K_T J_T \tilde{J}_C + \tilde{J}_C^T [\Delta J_{fa}^T \ \Delta J_{fp}^T] \tilde{J}_C. \quad (15)$$

Finally, the task space stiffness is calculated as

$$K_T = (\tilde{J}_C^T J_T^T)^+ \tilde{J}_C^T (K_q - [\Delta J_{fa}^T \ \Delta J_{fp}^T]) \tilde{J}_C (J_T \tilde{J}_C)^+ \quad (16)$$

Note that Eqn. (16) is always true whether the mechanism is subjected to an external force or not. In general, the task stiffness is a function of joint stiffness and the mechanism configuration. If there is no external force or the mechanism is in initial statue, f_T and f_C are zero. Then, the derivative of the Jacobian, $[\Delta J_{fa}^T \ \Delta J_{fp}^T]$, becomes a zero matrix. If we want to design the mechanism, we can assume that $[\Delta J_{fa}^T \ \Delta J_{fp}^T]$ is a zero matrix.

However, if an external force is exerted in the mechanism, f_T and f_C are not zero. This results in a configuration change, which effects the task space stiffness. If the mechanism interacts with the environment, the effect of $[\Delta J_{fa}^T \ \Delta J_{fp}^T]$ may be important.

If the mechanism is kinematically stable, i.e., J_{C_p} is square invertible, then

$$\tilde{J}_C = \begin{bmatrix} I \\ J_{C_p}^{-1} J_{C_a} \end{bmatrix}. \quad (17)$$

and Eqn. (15) becomes

$$K_{q_a} + J_{C_a}^T J_{C_p}^{-T} K_{q_p} J_{C_p}^{-1} J_{C_a} = J_{T_{comp}}^T K_T J_{T_{comp}}. \quad (18)$$

which is the same expression as obtained in [19].

DESIGN OPTIMIZATION

Design optimization involves selecting a set of design variables, p , to optimize one or more performance objectives subject to the constraints:

$$\min_p \{\mu_1, \mu_2, \dots\} \text{ subject to } \gamma_i(p) \leq \Gamma_i. \quad (19)$$

For this multi-objective optimization problem, we first find the Pareto optimal solutions [18], and then use them to guide the selection of the final design choice. A solution is Pareto when a feasible decrease in one design metric causes at least one other

design metric to increase. Solutions that are not Pareto are generally discarded because at least one design metric can be further improved with no cost to any of the other design metrics. The collection of all Pareto solutions is called the Pareto frontier. To facilitate visualization of design choices, usually only a small number of performance metrics (no more than 3) is considered in the optimization while the rest of the performance metrics are included in the constraints.

For flexure mechanism design, we choose the design variables to be the joint stiffness (which is determined by the joint geometry) and joint locations. The performance metrics are calculated with manipulability and stiffness, and the design constraints are calculated with flexure joint stress, mechanism size, and possibly others. Once the Pareto frontier is generated, e.g., by using the normal constraint method [20], secondary criteria such as performance sensitivity, dynamic characteristics, and manufacturability may be used to determine the final design parameters.

Flexure Joint Model

For a circular notch hinge type flexure joint (see Fig. 2), the joint stiffness is modeled as a pure rotation as given in [3]

$$K \approx \frac{2Ep}{9\pi} \sqrt{\frac{t^5}{R}}. \quad (20)$$

where E is the Young's Modulus of the hinge material, p is the depth of the joint, t the thickness of the thinnest portion of the joint, and R is the radius of the circle. A full 3D (planar translation and rotation) joint stiffness model is also given in [3].

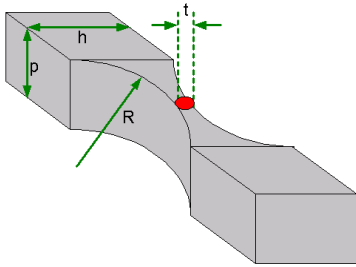


Figure 2. Circular Notch Joint

For a cantilevered joint (see Fig. 3), the joint stiffness may be approximately modeled as

$$K \approx 2\gamma K_\theta \frac{EI}{L}. \quad (21)$$

where E is the Young's Modulus, $I = \frac{pt^3}{12}$ is the moment of inertia about the axis perpendicular to the joint, L is the length of the

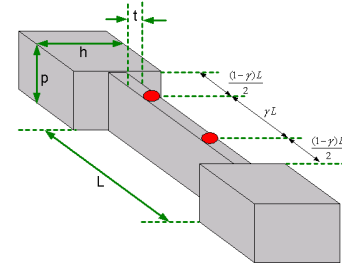


Figure 3. Cantilevered Joint

joint and γ and K_θ are experimentally determined constants [1]:

$$\gamma = 0.8517, K_\theta = 2.6762.$$

Maximum Joint Stress

The maximum stresses in the flexure joints are approximately proportional to the maximum deflections of these joints. For example, for a circular notch hinge joint with radius R , hinge width t , and Young's Modulus E , the maximum stress, σ_{\max} , is related to the angular deflection, θ_{\max} , by [3]

$$\theta_{\max} = \frac{3\pi}{4E} \sqrt{\frac{R}{t}} \sigma_{\max}. \quad (22)$$

For a cantilevered joint with length L and width t , the relationship is approximately, by [21]

$$\theta_{\max} = \frac{0.148 L}{E t} \sigma_{\max}. \quad (23)$$

If the maximum joint stress is given (e.g., from the yield stress of the material), it can be converted to an equivalent maximum joint displacement, $\Delta q_p^{(\max)}$ by using the above formulas. The maximum joint stress constraint can then be stated as a maximum deflection constraint:

$$|\Delta q_p| \leq \Delta q_p^{(\max)}. \quad (24)$$

Other Design Considerations

In addition to the performances measures mentioned above, other considerations may be needed to design the mechanism, such as the size of the mechanism, task space motion resolution (due to the motion resolution of the active joints), dynamic characteristics (bandwidth, resonant frequencies), sensitivity of performance with respect to manufacturing tolerance, etc.

EXAMPLE: NIST 1-D STAGE
Mechanism Architecture

A 1-degree-of-freedom (DOF) macro-scale precision motion stage using flexure joints was designed and fabricated by NIST [22, 23]. Several meso-scale (about the size of a credit card) models have also been built [24]. By replicating the design along the orthogonal axis, a 2-DOF version has also been designed and built. Such stages are currently being considered for deep space optical communication [25]. A schematic of the mechanism is shown in Fig. 4. A piezoelectric actuator transmits the y -axis motion through joints 1 and 4 to the two lower arms. These arms pivot about joints 2 and 5 and move the output stage through joints 3 and 6. To support the output stage (and to reduce angular crosstalk, i.e., undesirable angular motion), two additional arms also support the platform through joints 7-10. The goal of the design is to achieve desired manipulability (pure translation in y) and stiffness (large stiffness in the angular and x directions). The joints are constructed as circular notch joints (see [22]).

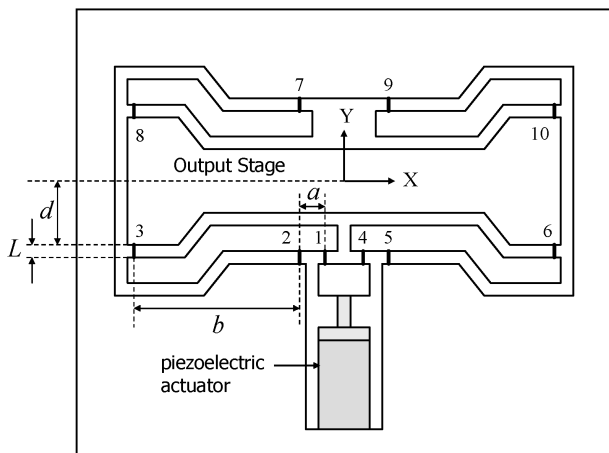


Figure 4. Configuration of NIST 1-D Mechanism

Using the proposed analysis tools and performance measures, our purpose is to reduce the size of 1-DOF NIST mechanism to the MEMS scale that has the same configuration. The overall size of mechanism must be less than $2.5\text{ mm} \times 2.5\text{ mm}$ including the active actuator.

To fabricate the micro scale parallel manipulator from the optimization results, 1 layer DRIE (Deep Reactive Ion Etching) process is used at MEMSCAP's SOIMUMPs process. On the Silicon On Insulator (SOI) wafer, the wet and dry etching processes are used to fabricate the $25\text{ }\mu\text{m}$ thickness structure. The DRIE process is shown in Fig. 5.

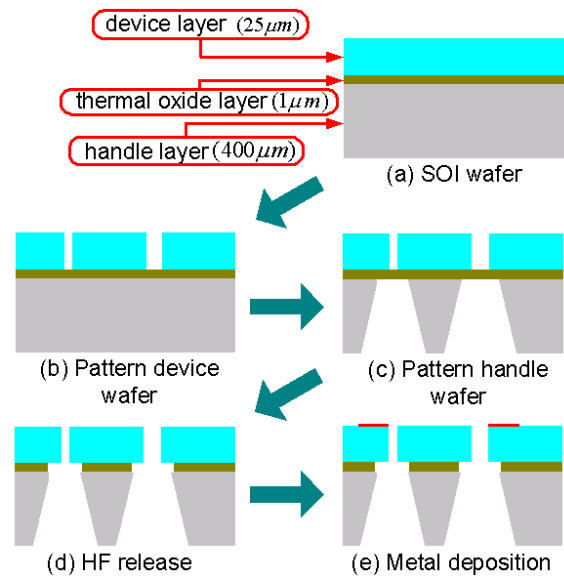


Figure 5. SOIMUMPs Process for NIST 1-DOF Manipulator

Kinematic Models

The mechanism consists of 6 kinematic chains constrained at the platform. This means that there are 15 total constraints (5 loops involving (x, y, θ)).

If all the joints in Fig. 4 are chosen to be idealized 1D rotational joints, then there are 10 passive DOF's and the mechanism is overconstrained (J_C is 15×10). Indeed, in this case, the mechanism cannot move from the equilibrium position shown. This means that the 1D joint approximation is not adequate to describe this mechanism. Therefore, we need a different joint model to describe this mechanism.

To illustrate the design procedure, we have considered the following joint model:

Replace joints 1, 3, 4, 6, 8, 10 by two rotational joints connected by a short rigid segment. The motivation of this assumption is to allow rotation as well as shear type of translation at these joints. Joints 2, 5, 7, 9 serve as pivots and are retained as pure rotational joints. In this case, there are 16 passive joints and 15 constraints, i.e., \tilde{J}_C is rank 2 (including one active joint). Since $J_T \tilde{J}_C$ (in Eqn. (15)) is rank 2, only the x - y components of K_T can be determined. Overall, the mechanism is underconstrained using this joint model.

The following sections discuss the optimal design structure depending on the different performance measure and the design variables.

Design Optimization for MEMS-scale Stage

For the MEMS-scale stage, the joints are made from a silicon-on-insulator (SOI) wafer. Silicon has different Young's Modulus depending on the crystal direction. The Young's Modulus is 129.5 GPa for [100], 168.0 GPa for [110], and 186.5 GPa for [111] from [26]. In this paper, we use $E = 160 \text{ GPa}$ which is the average value for the three different directions. The four quadrants of the stage are nominally all symmetric. We use the following dimensions as the initial stage values:

$$a = 100 \mu\text{m}, b = 1000 \mu\text{m}, L = 20 \mu\text{m}, d = 410 \mu\text{m}.$$

For circular notch joints, the passive joint stiffness is calculated using Eqn. (20) with $R = \frac{L}{2} = 10 \mu\text{m}$, $t = 5 \mu\text{m}$, $p = 25 \mu\text{m}$:

$$K_p = 5.00 \mu\text{N-m/rad}.$$

For cantilevered joints, the passive joint stiffness is calculated using Eqn. (21) with $t = 5 \mu\text{m}$, and $p = 25 \mu\text{m}$:

$$K_p = 9.50 \mu\text{N-m/rad}.$$

The actuator stiffness is obtained from the FEA simulation:

$$K_a = 30 \text{ kN/m}.$$

With the joint model, the task space Jacobian is (the task coordinate is arranged as (θ, x, y)):

$$J_{T_{comp}} = \begin{bmatrix} 0 \\ 0 \\ -10 \end{bmatrix}$$

showing only y -direction motion of the task frame.

The x - y portion of K_T is almost diagonal:

$$K_{T(x,y)} = \begin{bmatrix} 2.62 \times 10^5 & 9.06 \times 10^{-9} \\ 9.06 \times 10^{-9} & 453.24 \end{bmatrix} \text{ N/m}$$

with eigenvalues $(2.62 \times 10^5, 453.24)$.

For the maximum joint stress, we use the yield stress for silicon from [27]: $\sigma_{\max} = 7 \text{ GPa}$. However, this value may be chosen to be smaller to provide greater margin. The maximum stress constraint is imposed when the active joint is at its maximum extension

$$\Delta q_{a_{\max}} = 2 \mu\text{m}.$$

The joint stress formula Eqn. (22) is used for circular notch joints and Eqn. (23) is used for cantilevered joints. In this case, the maximum allowed joint deflection for the circular notch joint is 8.35° and for the cantilevered joint 1.48° .

Case A: Optimization for a, b, L To illustrate the design optimization procedure, three design parameters are chosen to be (a, b, L) with the bounds:

$$\begin{aligned} 33 \mu\text{m} &\leq a \leq 300 \mu\text{m}. \\ 333.3 \mu\text{m} &\leq b \leq 3000 \mu\text{m}. \\ 6.7 \mu\text{m} &\leq L \leq 60 \mu\text{m}. \end{aligned}$$

For multi-objective design metrics, we choose to maximize the manipulability (along y) and the relative stiffness between the x and y directions:

$$\text{Manipulability: } \mu_1 = \frac{10^2}{\|J_{T_{comp}}\|} \quad (25)$$

$$\text{Stiffness: } \mu_2 = \frac{10^4}{K_x/K_y}. \quad (26)$$

Note that the scaling constants are added to normalize between the two measures. The Pareto frontiers for cases A is shown in Fig. 6.

Case B: Optimization for a, b, L, t Including the flexure joint thickness, four design parameters are chosen to be (a, b, L, t) . The flexure joint thickness is bounded:

$$5 \mu\text{m} \leq t \leq 15 \mu\text{m}.$$

Using the same design metrics in case A, optimization is performed and the Pareto frontiers for cases B is shown in Fig. 7.

Case C: Optimization for L, t Based on the desired travel range of the mechanism, the range of the actuator and the range of motion amplification of the flexure mechanism are chosen. This sets the values for a and b . Then the flexure joint link (L) and thickness (t) are chosen for optimization. In case C, same design metrics are used as case A. The Pareto frontiers for cases C is shown in Fig. 8. In Fig. 8, first design metric, μ_1 , does not change during the optimization because the design variables can not effect the manipulability. Therefore, it is necessary to choose different design metrics for the multi-objective optimization. This is discussed in the case D.

Case D: Optimization for L, t with different design metrics In this case, using two design variables, different design metrics are chosen for the given displacement range. The optimization goal is to maximize the stiffness (along x direction) and to minimize the stiffness (along y direction):

$$\text{Stiffness } x: \mu_1 = \frac{1}{K_x} \times 10^4 \quad (27)$$

$$\text{Stiffness } y: \mu_2 = K_y \times 10^{-2}. \quad (28)$$

The Pareto frontier for cases D is shown in Fig. 9

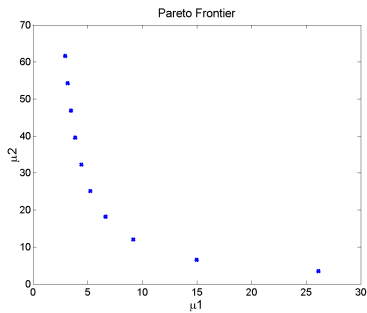


Figure 6. Pareto Frontier for Case A

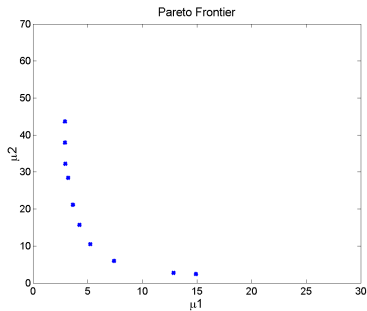


Figure 7. Pareto Frontier for Case B

Results for Meso-scale stage

The Pareto frontier shows all feasible solution areas in the design domain. Therefore, we can select the typical optimal design value by choosing the weight factor in the multi-objective design function. In this paper, we choose the equal weight when

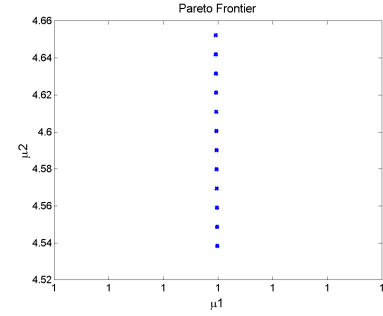


Figure 8. Pareto Frontier for Case C

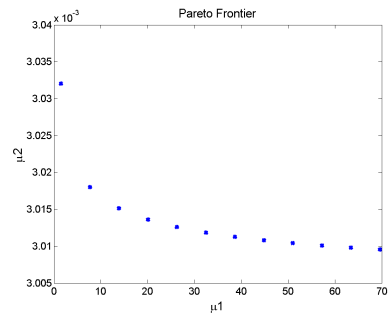


Figure 9. Pareto Frontier for Case D

Table 1. Optimal Values for Design Variables

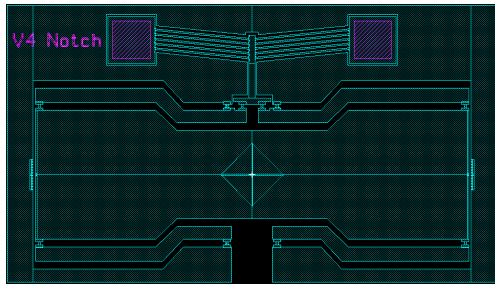
	Initial value	Optimal value		
		Case A	Case B	Case D
a	$100 \mu\text{m}$	$115.7 \mu\text{m}$	$97.602 \mu\text{m}$.
b	$1000 \mu\text{m}$	$1200 \mu\text{m}$	$1200 \mu\text{m}$.
L	$20 \mu\text{m}$	$18.135 \mu\text{m}$	$21.824 \mu\text{m}$	$55 \mu\text{m}$
t	$7 \mu\text{m}$.	$12.261 \mu\text{m}$	$5.52 \mu\text{m}$

the two performance indices are considered with same amount:

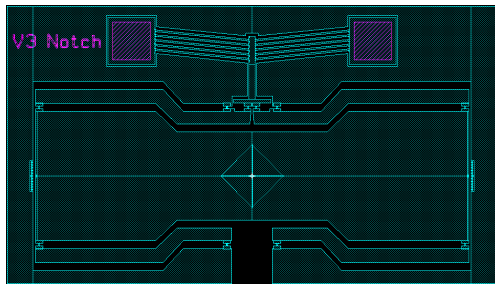
$$\mu = 0.5\mu_1 + 0.5\mu_2.$$

The optimal design values for Case A, B, and D are summarized in Table 1. In each case, the angular deformation of passive joints is less than the maximum deflection range, when the active joint is $2 \mu\text{m}$. Therefore, the maximum deflection constraint for the circular notch joints and the cantilevered joints are satisfied for all cases.

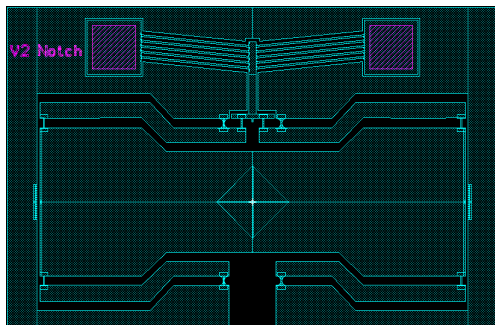
Finally, the optimal structure is design for the SOIMUMPs process shown in Fig. 10.



(a) Case A



(c) Case B



(e) Case D

Figure 10. Design Structures for SOIMUMPs Process

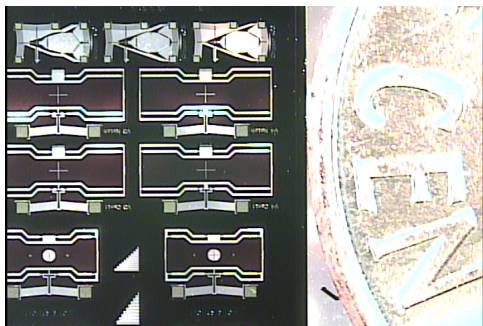


Figure 11. Fabricated NIST 1D Stages

Active Actuator Design

Since the size of the manipulator is limited, the actuator must be as small as possible. The actuator mechanism must be a planar structure because of the DRIE process. By considering these criteria, thermal actuators are designed to actuate the active flexure joints. Thermal actuators can generate relatively large forces compared to other MEMS actuators, such as electro-static actuators. The length of the actuator is $500\ \mu\text{m}$ and the width is $10\ \mu\text{m}$. Using the basic structure of one actuator, we stacked up multiple actuators using the long-common beam between actuators that will increase the force to the MEMS structure. The thermal actuator was fabricated using the DRIE and its FEA simulation are shown in Fig. 12.

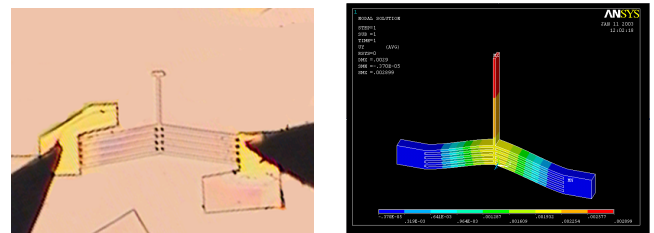


Figure 12. Active Joint Actuator using Thermal Mechanism

FUTURE WORK AND CONCLUSION

In this paper, we have presented analysis and design tools for MEMS parallel mechanisms with lumped flexure joints. We pose the design problem as a multi-objective optimization with manipulability and stiffness as performance measures and constraints. A 1-D MEMS stage is designed as an example to illustrate the modeling and design approach.

The various MEMS mechanism designs described in this paper have been sent to the MEMS foundry and been fabricated successfully. We will conduct experimental trials to determine the validity of the proposed analysis tool and performance measures. It will be discussed in future publications

REFERENCES

- [1] Howell, L., 2001. *Compliant Mechanisms*. John Wiley and Sons, Inc.
- [2] Kota, S., 2000. "Compliant systems using monolithic mechanisms". *Smart Material Bulletin*, **7-9** [Mar.].
- [3] Smith, S., 2000. *Flexure: Elements of Elastic Mechanisms*. Gordon and Breach Science Publishers.
- [4] Kota, S., Joo, J., Li, Z., Rodgers, S., and Sniegowski, J., 2001. "Design of compliant mechanisms: Applications to

- mems". *Analog Integrated Circuits and Signal Processing*, **29** [Oct.], pp. 7–15.
- [5] Ananthasuresh, G., and Frecker, M., 2001. "Optimal synthesis with continuum models". In *Compliant Mechanisms*, L. Howell, Ed. John Wiley and Sons, Inc., Chapter 9, pp. 301–336.
- [6] Culpepper, M., and Anderson, G., 2003. "Design of a low-cost nano-manipulator which utilizes a monolithic, spatial compliant mechanism". *Submitted to the Journal of Precision Engineering* []. URL <http://psdam.mit.edu/publications.html>.
- [7] Pham, H., and Chen, I.-M., 2003. "Optimal synthesis for workspace and manipulability of parallel flexure mechanism". In 11th World Congress in Mechanism and Machine Science.
- [8] Loncaric, J., 1985. *Geometrical Analysis of Compliant Mechanisms in Robotics*. PhD Thesis, Harvard University, Cambridge, MA.
- [9] Huang, S., and Schimmels, J. M., 1998. "Achieving an arbitrary spatial stiffness with springs connected in parallel". *ASME Journal of Mechanical Design*, **120** (4) [Dec.], pp. 520–526.
- [10] Ciblak, N., and Lipkin, H., 1998. "Synthesis of stiffness by springs". In Proceedings of 1998 ASME Design Engineering Technical Conferences.
- [11] Roberts, R., 1999. "Minimal realization of a spatial stiffness matrix with simple springs connected in parallel". *IEEE Transaction on Robotics and Automation*, **15** (5) [Oct.], pp. 953–958.
- [12] Sugar, T., and Kumar, V., 2002. "Design and control of a compliant parallel manipulator". *ASME Journal of Mechanical Design*, **124** (4) [Dec.], pp. 676–683.
- [13] Lou, Y., Liu, G., and Li, Z., 2003. "Optimal design of parallel manipulators via LMI approach". In Proceedings of the 2003 IEEE International Conference on Robotics and Automation, vol. **2**, pp. 1869–1874.
- [14] Merlet, J.-P., 2003. "Determination of the optimal geometry of modular parallel robots". In Proceedings of the 2003 IEEE International Conference on Robotics and Automation, vol. **1**, pp. 1197–2002.
- [15] Yoshikawa, T., 1985. "Manipulability of robotic mechanisms". *International Journal of Robotics Research*, **4** (2) [Summer], pp. 3–9.
- [16] Wen, J. T., and Wilfinger, L. S., 1999. "Kinematic manipulability of general constrained rigid multibody systems". *IEEE Transactions on Robotics and Automation*, **15** (3) [Jun.], pp. 558–567.
- [17] Bicchi, A., and Prattichizzo, D., 1998. "Manipulability of cooperation robots with passive joints". In Proc. 1997 IEEE Int. Conf. on Robotics and Automation, pp. 1038–1044.
- [18] Ismail-Yahaya, A., and Messac, A., 2001. "Required relationship between objective function and pareto frontier orders: practical implications". *American Institute of Aeronautics and Astronautics Journal*, **39** (11) [], pp. 2168–2174.
- [19] Alici, G., and Shirinzadeh, B., 2003. "Kinematics and stiffness analyses of a flexure-jointed planar micromanipulation system for a decoupled compliant motion". In Proceedings of the 2003 IEEE/RSJ Intl. Conference on Intelligent Robots and Systems, vol. **4**, pp. 3282–3287.
- [20] Ismail-Yahaya, A., and Messac, A., 2002. "Effective generation of the pareto frontier using the normal constraint method". In 40th Aerospace Sciences Meeting and Exhibit.
- [21] Henein, S., 2000. *Conception des Structures Articulees a Guidages Flexibles de Haute Precision*. PhD Thesis, Ecole Polytechnique Federale de Lausanne, Lausanne, EPFL.
- [22] Amatucci, E., Dagalakis, N., Kramar, J., and Scire, F., 2000. "Performance evaluation of a parallel cantilever bi-axial micropositioning stage". In Proc. of the American Society of Precision Engineering, 15th Annual Meeting.
- [23] Dagalakis, N., Kramar, J., Amatucci, E., and Bunch, R., 2001. "Kinematic modeling and analysis of a planar micropositioner". In Proc. of the American Society of Precision Engineering, 16th Annual Meeting.
- [24] Gorman, J., Dagalakis, N., and Boone, B., 2003. "Multi-loop control of a nanopositioning mechanism for ultra-precision beam steering". In Free-Space Laser Communication and Active Laser Illumination III, SPIE Vol. 5160, pp. 170–181.
- [25] Boone, B., Bokulic, R., Andrews, G., McNutt, R., Jr., and Dagalakis, N., 2002. "Optical and microwave communications system conceptual design for a realistic interstellar explorer". In Proceedings of the 47th Annual SPIE Meeting.
- [26] Kasper, E., 1995. *Properties of Strained and Relaxed Silicon Germanium*. INSPEC.
- [27] Madou, M. J., 2002. *Fundamentals of Microfabrication, 2nd edition*. CRC.